



Lateral pressure on pile foundations in cohesive soils due to horizontal soil movements

Jörg Bauer¹ · Oliver Reul²

Received: 2 March 2023 / Accepted: 21 November 2023 / Published online: 17 April 2024
© The Author(s) 2024

Abstract

In soft soil layers, piles are frequently loaded laterally by horizontal soil movements. In many cases, the lateral pressure acting on piles due to horizontal soil movements is calculated with empirically or analytically based approaches, respectively. However, most of these design approaches do not consider possible influences on the resulting pile loads. This paper presents the results of model tests and numerical simulations on single piles and pile groups in cohesive soil subjected to lateral loads which were carried out to overcome limitations of available design approaches. Based on extensive small-scale $1 \times g$ -model tests and numerical investigations with the finite element method, influencing factors on the lateral pressure, such as the roughness of the pile–soil interface, the pile size, the pile shape and the pile spacing were identified. A parametric study with the numerical model quantified the most relevant factors influencing the development of lateral pressure on piles due to adjacent surface loads and lead to the development of a simplified analysis approach.

Keywords Horizontal loaded piles · Model tests · Numerical analysis · Pile foundations · Soft soil · Soil movements

List of symbols

a_p	Edge length of a pile
c'	Effective cohesion of the soil of the Hardening Soil-Model
d_p	Diameter of a pile
d_q	Distance between the pile and the surface load
E	Young's modulus of structural components (piles and pile cap)
E_S	Confined stiffness modulus of the soil
E_{50}^{ref}	Reference stiffness modulus of the hardening soil model
$E_{\text{ur}}^{\text{ref}}$	Reference Young's modulus for unloading–reloading of the Hardening Soil-Model
g	Acceleration of gravity
h_w	Thickness of the cohesive soil layer

L_p	Length of a pile
m	Power for the stress level dependency of stiffness in the Hardening Soil-Model
P	Lateral pressure on the pile as linear distributed load
P_{ult}	Ultimate lateral pressure on the pile as linear distributed load
p	Lateral pressure on the pile
p_{mean}	Average value of the lateral pressure along the pile shaft
p_{ult}	Ultimate lateral pressure on the pile
p^{ref}	Reference confining pressure of the Hardening Soil-Model
q	Surface load in the finite element model
q_{ult}	Ultimate capacity of a strip foundation
R_f	Failure ratio of the Hardening Soil-Model ($R_f = 0.9$)
R_{inter}	Interface shear strength ratio for the modelling of soil-structure interaction
s	Pile spacing of group piles
s_u	Undrained shear strength of the soil
v	Displacement rate of the soil flowing around the pile
γ	Unsaturated weight of the soil
γ_{sat}	Saturated weight of the soil

✉ Oliver Reul
o.reul@uni-kassel.de

Jörg Bauer
joerg.bauer@baw.de

¹ Department of Geotechnical Engineering, Federal Waterways Engineering and Research Institute (BAW), Kussmaulstraße 17, 76187 Karlsruhe, Germany

² Department of Geotechnical Engineering, University of Kassel, Mönchebergstraße 7, 34109 Kassel, Germany

δ	Relative displacement between the pile and the soil body
χ_{GP}	Pile group factor after Eq. 5
χ_{dq}	Coefficient for the distance between a pile and a surface load after Eq. 4
μ	Degree of utilisation of the strip foundation
ν	Poisson's ratio of the soil
ν_{ur}	Poisson's ratio for unloading–reloading of the soil
φ'	Effective friction angle of the soil of the Hardening Soil-Model
χ	Empirically or theoretically derived coefficient after Eq. 1
ψ	Angle of dilatancy of the soil

- the size of the pile cross section,
- the pile shape,
- pile group effects.

Neglecting these parameters, in design practice, frequently the following simplified expression is applied to define the ultimate lateral pressure P_{ult} for the ultimate limit state:

$$P_{ult} = \chi \cdot s_u \cdot d_p \text{ or } P_{ult} = \chi \cdot s_u \cdot a_p \quad (1)$$

where χ is an empirically or theoretically derived coefficient, s_u is the undrained shear strength, d_p is the pile diameter and a_p is the edge length of the pile. Table 1 gives an overview on the range of values for the coefficient χ defined in the literature.

However, it can be assumed that in many practically relevant cases the ultimate lateral pressure will not be reached since the bearing capacity of the strip foundation is significantly higher than the surface load causing the horizontal soil movements and the loading rate is relatively small. Therefore, for the estimation of the resulting lateral pressure for pile design pre-failure conditions appear to be decisive with the influences of the parameters mentioned above on the relative displacement between pile and soil being largely unknown.

The European standard on geotechnical design EC 1997-1 (EC7-1) [17] requires proof against the effects caused by lateral pressure, but does not specify an analysis method to quantify these effects. In the German supplementary rules to the EC7-1, DIN EN 1997-1 (DIN 1054)

1 Introduction

In soft soil layers, piles are frequently loaded laterally by horizontal soil movements caused by eccentric loading or unloading of the ground surface around the piles (Fig. 1). According to [14] piles subjected to such a lateral pressure are termed “passive piles”, while piles subjected to horizontal loads at the pile head caused by the superstructure are termed “active piles”.

In many cases, the lateral pressure acting on piles due to horizontal soil movements is calculated with empirical approaches or analytically based on plasticity or earth pressure theory, respectively. [35] classify design methods for piles subjected to lateral loads as

- empirical methods,
- pressure-based methods,
- displacement-based methods,
- finite element analyses.

Previous studies (e.g. [3, 18, 21, 23, 30]) indicate that the lateral pressure on piles depends on various parameters such as

- the roughness of the pile–soil interface,

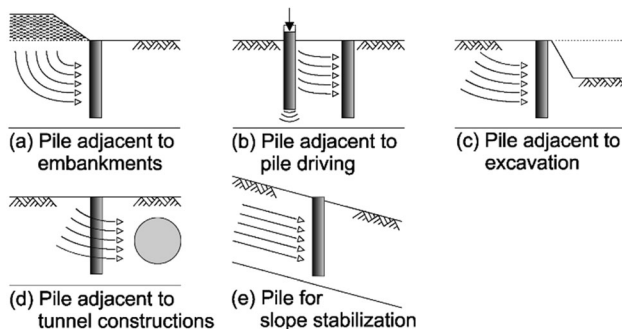


Fig. 1 Lateral pressure on piles due to horizontal soil movement (after [13])

Table 1 Coefficient χ for the estimation of the lateral pressure P_{ult}

Reference	Principle of derivation	χ
		–
[39]	Model tests	8.28 (square pile)
[32]	Theoretical	2.60 (circular pile) 3.40 (square pile)
[40]	Theoretical	11.42
[18]	Theoretical	4.50
[30]	Theoretical	9.14 (“smooth” circular pile) 11.94 (“rough” circular pile)
[13]	Finite element analysis	11.40 (square pile)
[10]	Finite element analysis	11.75 (square pile)
[27]	Model tests	10.50 (circular pile)
[12]	Finite element analysis	9.11 (“smooth” circular pile) 11.94 (“rough” circular pile)
[23]	Model tests	10.60 (square pile)
[21]	Model tests	8.33 (square pile) 8.62 (circular pile)
[15]	Theoretical	7.00

[16], for the calculation of the lateral pressure reference is made to the Recommendations on Piling (DGGT 2014 [15]) listed in Table 1.

As part of a research project to overcome some of the limitations mentioned above this paper presents the results of $1 \times g$ model tests and of a numerical parametric study on piles subjected to lateral pressure which led to the development of an improved analysis approach.

2 $1 \times g$ Model tests

2.1 Test set-up

The $1 \times g$ model tests in Kaolin clay comprised 25 tests on single piles and 11 tests on pile rows with up to 3 piles. In all tests, the soil was flowing around fixed single piles or pile rows, respectively, while the following parameters were varied:

- shear strength s_u of the Kaolin clay ($s_u = 0.6$ kPa to $s_u = 5.2$ kPa),
- pile shape (circular and square cross section, respectively),
- pile diameter d_p or edge length a_p (20 mm, 30 mm and 40 mm),
- roughness of the pile–soil interface (“smooth” piles and “rough” piles, respectively),
- displacement rate v of the soil flowing around the pile ($v = 0.01$ mm/min to $v = 1.00$ mm/min)
- pile spacing s in the pile group tests ($s = 2 \cdot d_p$ to $s = 10 \cdot d_p$)

Figure 2 shows the test set-up. The soil is located in a box on a cart which is pulled displacement controlled by means of a hydraulic press which is connected to the cart by means of a steel cable with ball bearings at both ends. During the tests, each model pile was fixed by means of two guyings aligned with the direction of the soil movement. The guyings, a steel cable connected to a load cell which allowed for the measurement of forces, were connected with the back of the pile near the pile head and the pile base, respectively. The 200 mm long model piles were fabricated from aluminium profiles with circular or square cross sections, respectively. The plain surfaces of the aluminium profiles are considered as “smooth” in the scope of this work. For the investigation of “rough” piles, sandpaper was glued on the aluminium profiles.

For the model tests kaolin clay was used to ensure a high reproducibility of the tests [7]. The kaolin clay with a very soft consistency and water content close to the liquid limit or even higher yielding a liquidity index $I_L \geq 1$ was placed in ~ 3 cm thick layers in the box. Every layer was smoothed before the next layer was placed to minimise

inclusions of air in the clay. Under the assumption that the structure of kaolin clay does not change significantly during consolidation [34] and to proceed with the testing programme in a reasonable time frame, the tests started immediately after the soil placement—that is, no time was given for consolidation under self-weight. The undrained shear strength was determined in the test box in preliminary tests and after each test with a small vane penetrometer at 30 to 40 locations in the test box. Immediately after each test at six locations in the test box, soil samples were taken to determine the water content and the uniformity of the soil installation was controlled by means of a small-scale cone penetration test [7]. Based on extensive preliminary tests, the relationship between the water content and the undrained shear strength of the kaolin clay was well established and was confirmed during the tests. With the water contents of the kaolin clay varying between $w = 34\%$ and $w = 50\%$ during the tests, undrained shear strength between $s_u = 0.6$ kPa and $s_u = 5.2$ kPa were achieved. The properties of the Kaolin clay are summarised in [7].

The tests were analysed with the PIV-Method (e.g. [41]) using dispersed fine sand as a tracer on top of the Kaolin clay surface. Based on the PIV observations, the zone of deforming soil around the piles did not extend to the container boundaries. [7] provide a detailed documentation of test set-up, soil properties and sample preparation.

2.2 Test results

In the scope of this paper, the lateral pressure acting on the pile p and the relative displacement between the pile and the soil body δ were normalised by the undrained shear strength s_u and the pile diameter d_p or pile edge length a_p , respectively. The relative displacement between pile and soil body δ was assumed to be equivalent to the displacement of the box. The lateral pressure of the pile p was derived from the measured forces on the pile P divided by the pile length h_w and the pile diameter d_p or pile edge length a_p , respectively:

$$p = P / (h_w \cdot d_p) \text{ or } p = P / (h_w \cdot a_p) \quad (2)$$

Similar to the work published by [23, 27, 28], the model tests were carried out up to a maximum relative displacement of $\delta/d_p \approx \delta/a_p \approx 1$ which is also assumed to be a value that in engineering practice usually will not be exceeded. Therefore, the model tests focus on pre-failure conditions since the ultimate lateral pressure acting on the pile was not reached in the current model tests.

All results presented in the scope of this paper were derived from tests with a displacement rate of the soil

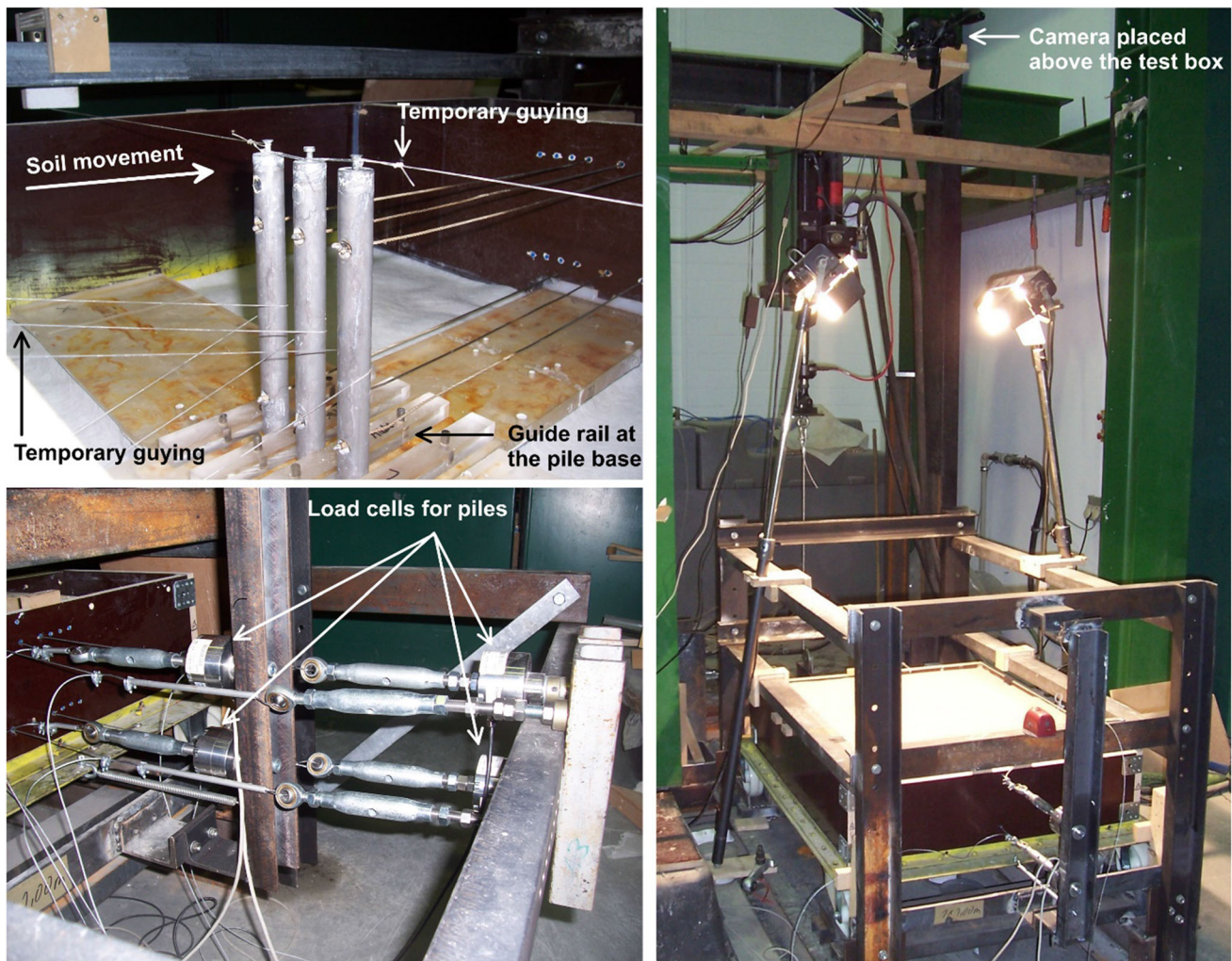
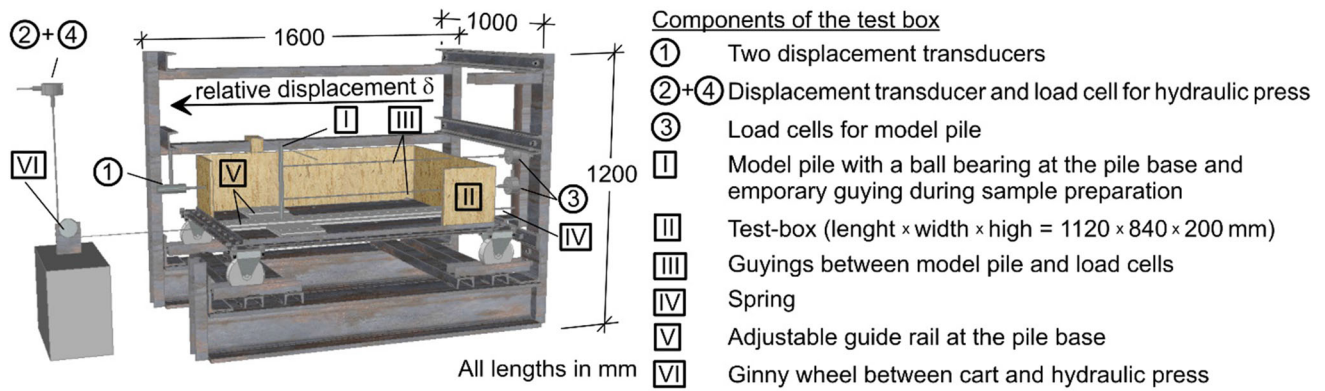


Fig. 2 Test set-up of the model tests

flowing around the pile of $v = 0.1$ mm/min. [7] discuss the influence of the displacement rate on the lateral pressure.

Figure 3 shows the results of the PIV analysis of two tests with an undrained shear strength $s_u \approx 2.2$ kPa ($d_p = 40$ mm) and $s_u \approx 5.2$ kPa ($d_p = 30$ mm), respectively, for a relative displacement between pile and soil, i.e. the displacement of the box, of $\delta \approx 0.1 \cdot d_p$. The PIV analyses

were carried out up to a relative displacement of $\delta \approx 1.0 \cdot d_p$. For $s_u \leq 1$ kPa generally a flow around the soil could be observed in the model tests [4]. For $s_u \approx 2$ kPa, a gap developed behind the piles with relative displacements increasing $\delta \geq 0.2 \cdot d_p$. For $s_u \approx 5$ kPa, the gap developed immediately with the start of the test. This gap extended over the complete length of the pile which is in agreement

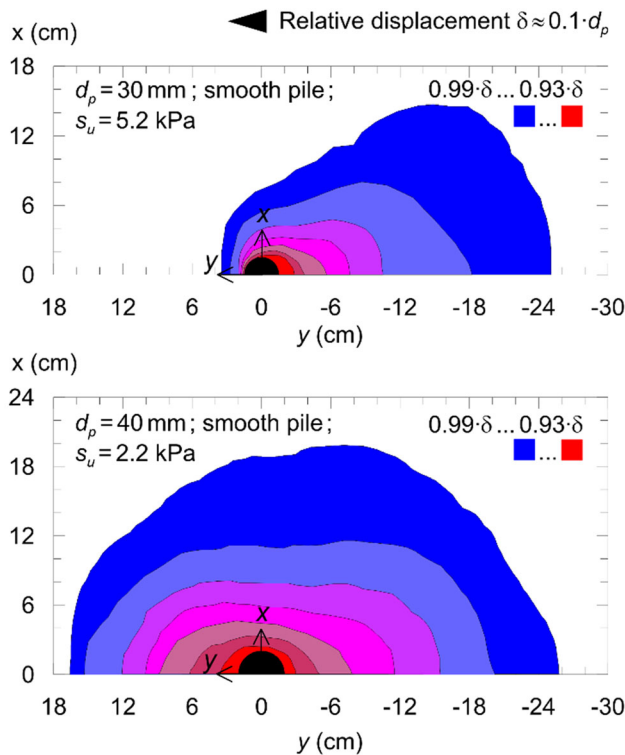


Fig. 3 Model tests—contour lines of the displacement of the soil surface derived from the PIV-analysis for single piles

with earth pressure theory [4]. However, due to the significantly higher stresses in the soil, gaps of this size will not occur at large-scale piles. The magnitude of the undrained shear strength also influenced the pattern of soil movement adjacent to the pile.

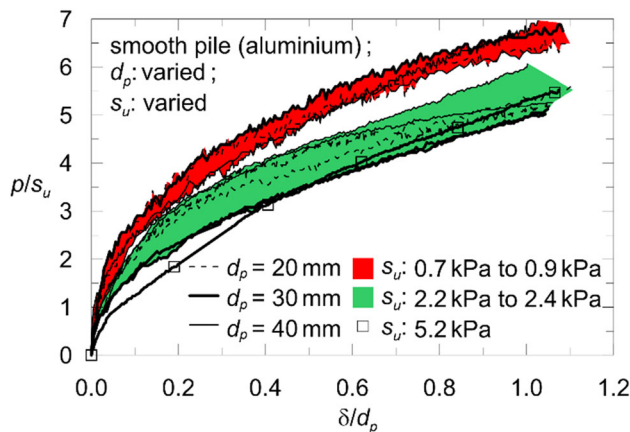


Fig. 4 Models tests—variation of the normalised pressure acting on piles p/s_u with normalised relative displacement δ/d_p ; Influence of the pile diameter d_p and shear strength of the soil s_u

Figure 4 shows the variation of normalised soil displacement δ/d_p with the normalised pressure acting on the piles p/s_u for smooth circular piles. On the one hand, the tests exhibited increased values for p/s_u for lower values of s_u . This can be explained with the different patterns of soil movement adjacent to the piles (Fig. 3) where soil flow around the piles yields higher lateral pressures than an accumulation of soil in front of the piles. On the other hand, the tests show no significant influence of the pile size on the pressure p which might be explained by the very small size of the piles in the model tests [7].

Figure 5 shows a comparison of test results for smooth piles and rough piles for an undrained shear strength of $s_u = 0.8$ kPa and $s_u = 2.4$ kPa, respectively. The rough piles exhibit lateral pressures 19–32% higher than the smooth piles. Moreover, it appears that the difference between smooth and rough piles is more pronounced for higher values of s_u . This test result corresponds with the analytical solution by [30] predicting an ultimate pressure p for a perfectly rough pile approximately 30% higher than for a perfectly smooth pile.

Figure 6 compares pile rows with two piles perpendicular to the soil movement with varying pile spacing where the lateral pressure was measured for each pile separately and then averaged. For a spacing of $s \leq 8 \cdot d_p$, the lateral pressure acting on the piles in the row is smaller than the lateral pressure on a comparable single pile. In general, the investigations show the lateral pressure decreasing with decreasing pile spacing. Similar results as in the current model tests were presented by [23, 28].

Apart from the main research project [4], additional tests results are documented in [6, 7].

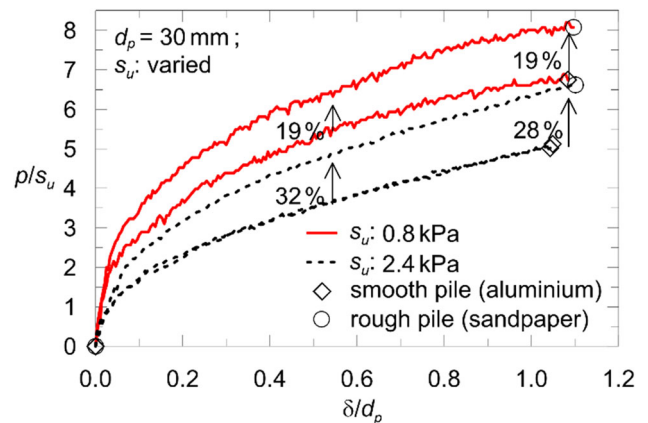


Fig. 5 Model tests—variation of the normalised pressure acting on piles p/s_u with normalised relative displacement δ/d_p ; Influence of the pile roughness

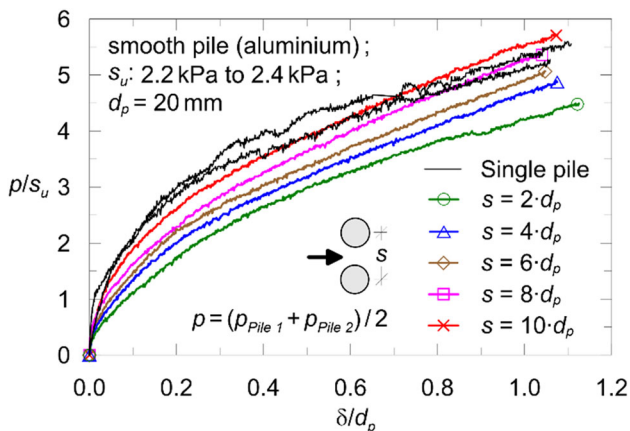


Fig. 6 Model tests—variation of the normalised pressure acting on piles p/s_u with normalised relative displacement δ/d_p ; Pile rows with two piles and varied pile spacing

3 Numerical parametric study

3.1 Preliminary remarks

The aim of the numerical parametric study based on the finite element method was to systematically quantify the influencing parameters on the lateral pressure and to develop a simplified analysis approach applicable for engineering practice which considers these parameters. Since the shear strength and stiffness of the soil in the aforementioned $1 \times g$ model tests are not comparable with in situ soil conditions, the back analysis of the $1 \times g$ model tests was used to show the general suitability of the numerical model to simulate lateral pressure on piles [8], i.e. the $1 \times g$ model tests were not applied for the determination of design parameters for the prototype scale. The further verification of the numerical model then comprised the back analysis of in situ measurements [4, 31]. The suitability of the finite element method simulating the lateral pressure on piles was also confirmed by e.g. [20, 26, 37].

The results presented by [8] showed a good agreement between the model tests and numerical back analyses, which was carried out by means of total stress finite element analysis with undrained shear parameters on one hand and effective stress analysis with effective shear parameters on the other. The numerical parametric studies on single piles confirmed the significant influence of the undrained shear strength, the pile shape, the pile diameter and the roughness of the pile–soil interface on the normalised lateral pressure. The numerical back analysis of pile groups with piles lined up perpendicular or longitudinal, respectively, to the direction of the soil movement showed diminishing group effects with increasing pile spacing. It is interesting to note that [2, 3] also achieved

good agreement with the model tests by [6, 7] as well as with the results of the finite element analysis by [8] carrying out numerical simulations with the Convected Particle Domain Interpolation (CPDI1). The CPDI1 is a further development of the material point method (MPM) and can be used to simulate very large deformations in the soil (e.g. [1, 19]).

Reul et al. [31] present the back analysis of a large-scale test on a pile group in cohesive soil subjected to lateral pressure documented by [25] by means of 3D finite element coupled pore pressure–displacement analyses. A reasonable agreement between the measured bearing behaviour of the pile foundation, and the finite element analysis was achieved. Especially the consolidation process and the creep deformations, which were modelled by means of a visco-hypoplastic soil model were reproduced well in the finite element analysis. Additionally, [4] presents the back analyses of a large-scale test documented by [38] and centrifuge tests documented by [10].

3.2 Finite element model

The numerical parametric study presented in this research work was carried out with the system and boundary conditions shown in Fig. 7, and the 3D finite element models shown in Figs. 8 and 9. The soil and the piles are represented by 15-order solid finite elements of wedge shape. The circular piles were replaced by dodecagonal cross sections with approximately the same shaft circumference.

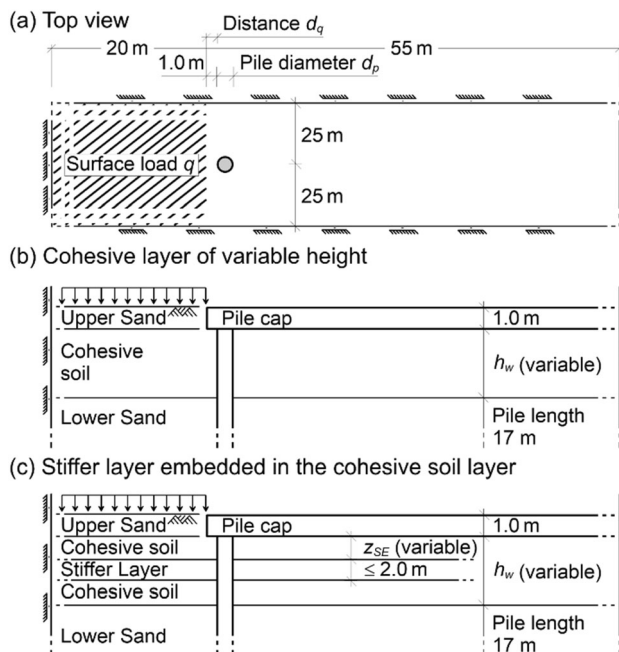


Fig. 7 System and boundary conditions for the investigations on single piles

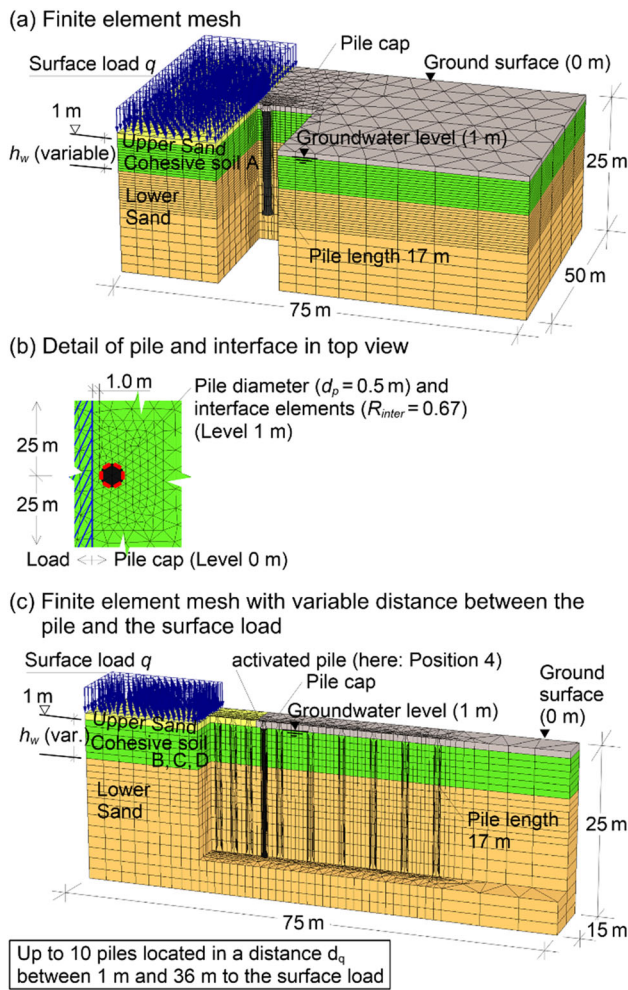


Fig. 8 Finite element model for the investigations on single piles

Contact between soil and piles was modelled using interface elements (Fig. 8b).

The soil stratigraphy comprises an upper sand layer with a thickness of 1.0 m underlain by a cohesive soil layer with the thickness h_w varying in the parametric study. The cohesive soil layer is followed by a lower sand layer which extends down to the bottom surface of the model. The groundwater level is located at the top of the cohesive soil layer.

The lateral pressure acting on the piles is caused by a fully flexible vertical load located at ground level. A pile cap with a thickness of 1.0 m was placed above the piles which extends to the horizontal model boundaries. Preliminary studies showed no significant influence of the size of the pile cap on the lateral pressure acting on a pile group [4].

Pile length were held constant at $L_p = 17.0$ m. For the investigations with the finite element model shown in Fig. 8a, the following parameters were varied:

- shear strength s_u of the cohesive soil (4–36 kPa),

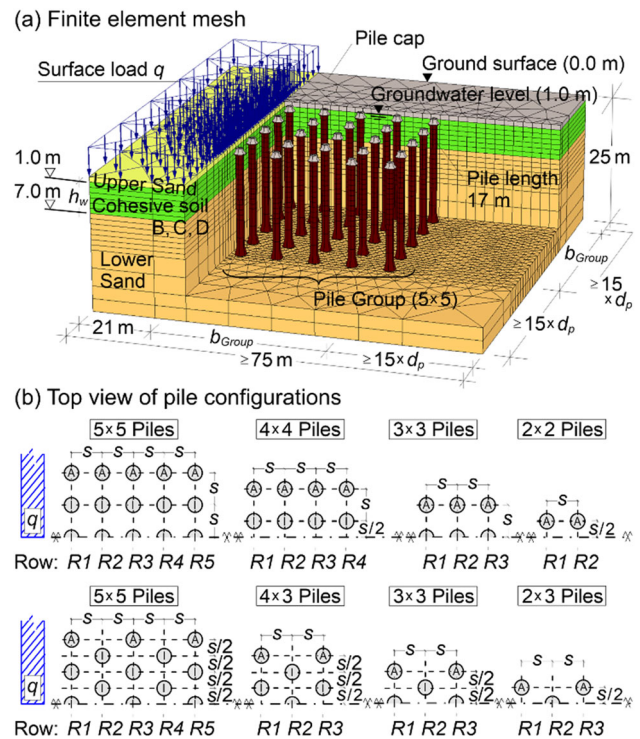


Fig. 9 Finite element model for the investigations on pile groups

- stiffness E_S of the cohesive soil (0.1–11 MPa),
- thickness of the cohesive soil layer h_w (1.0–12.0 m),
- pile shape (circular and square cross section, respectively),
- pile diameter d_p or edge length a_p (0.3–3.0 m),
- roughness of the pile–soil interface (“smooth” piles and “rough” piles, respectively).

Based on the configuration shown in Fig. 8a, the effect of a significantly stiffer layer embedded in the cohesive soil layer was further investigated (Fig. 7c). For this purpose, the shear strength s_u and the stiffness E_S of the cohesive soil layer as well as the depth of the significantly stiffer layer z_{SE} were varied in the bandwidth mentioned above with the thickness of the significantly stiffer layer ranging between 0.5 and 2.0 m [4].

In the investigations for single, rough piles the distance between the pile and the surface load was varied between 1.0 and 36.0 m (Fig. 8c).

The parametric study for pile groups was carried out for groups of 2×2 , 2×3 , 3×3 , 4×3 , 4×4 and 5×5 piles (Fig. 9b) with the piles spacing varying between $s = 3 \cdot d_p$ to $s = 9 \cdot d_p$.

The material behaviour of the sand layers (incl. a significantly stiffer layer with the material parameters of the upper sand embedded in the cohesive soil layer) was modelled with a linear elastic-perfect plastic soil model applying the Mohr–Coulomb failure criteria and a

nonassociated flow rule for the plastic deformations. Preliminary studies varying the material parameters of the sand layers showed no significant influence on the lateral pressure. For the results presented in the scope of this paper, the material behaviour of the cohesive soil layer was modelled with the Hardening Soil-Model [11]. The influence of creep deformations on the lateral pressure was investigated by [4] and is not in the focus of this paper.

Interface elements with a linear elastic-perfect plastic material behaviour were applied for the simulation of the pile–soil interaction. For the applied Mohr-Coulomb failure criteria, the shear parameters of the surrounding soil were used. For the remainder of this paper, piles with an interface shear strength ratio of $R_{\text{inter}} = 0.33$ are termed “smooth” and for an interface shear strength of $R_{\text{inter}} \geq 0.67$ are termed “rough”. If not indicated otherwise all results presented in the scope of this paper were derived for an interface shear strength ratio $R_{\text{inter}} = 0.67$, i.e. for rough piles.

The piles and the pile cap are considered to behave linear elastically. The material parameters applied in the finite element analyses are summarised in Tables 2, 3 and 4.

Preliminary studies carried out for undrained conditions and drained conditions under consideration of consolidation processes showed that undrained conditions yield the maximum lateral pressure decisive for pile design [4]. In the scope of the parametric study presented in this paper, undrained conditions were considered.

The finite element analysis included the following steps:

1. Generation of the in situ stress state.
2. Installation of the piles using the “wished-in-place” technique, i.e. no changes in the soil surrounding the piles caused by the installation process were modelled.
3. Application of the load.

The first two analysis steps were carried out under drained conditions while during the application of the load in step 3 undrained conditions were considered resulting in the buildup of excess pore pressure.

The results of the parametric study are evaluated by means of the constrained stiffness modulus E_S and the undrained shear strength s_u both acting in the in situ stress state. The mean value of the constrained stiffness modulus

for the cohesive soil layer (Fig. 10a) was derived from the material parameters of the Hardening Soil-Model (Table 3) applying the approach suggested by [11]:

$$E_S \approx E_{50}^{\text{ref}} \left(\frac{c' \cdot \cos \varphi' - \sigma'_y \cdot \sin \varphi'}{c' \cdot \cos \varphi' + p^{\text{ref}} \cdot \sin \varphi'} \right)^m \quad (3)$$

where E_{50}^{ref} is the reference stiffness modulus corresponding to the reference confining pressure $p^{\text{ref}} = 0.1$ MPa and m is the power for the stress level dependency of stiffness.

The mean value of the undrained shear strength for the cohesive soil layer was derived from numerical simulations of undrained triaxial tests as indicated in Fig. 10b applying the drained shear parameters φ' and c' of the Hardening Soil-Model (Table 3).

Due to the boundary conditions and the pile cap considered in the finite element models (Figs. 8, 9), the load q can be significantly higher than the ultimate capacity of a comparable strip foundation q_{ult} (Fig. 11b). The soil then reaches its ultimate capacity in the vicinity of the piles with the ultimate lateral pressure p_{ult} acting on the piles (Fig. 11a). Therefore, the numerical model applying loads $q > q_{\text{ult}}$ yield higher lateral pressures, i.e. a conservative design approach, than what can be expected under boundary conditions typical for engineering practice. For the evaluation of the parametric study again, the mean value of the lateral pressure is considered (Fig. 12).

The ultimate capacity for the strip foundation was established by means of a φ – c -reduction for a system without piles and the pile cap replaced by the upper sand layer. If not mentioned otherwise, all results presented in the scope of this paper were derived for $q = q_{\text{ult}}$.

3.3 Results of the numerical study for single piles

Figure 13 shows the variation of the normalised pressure acting on the piles, p_{mean}/s_u , with the normalised surface load q/q_{ult} for the basic model (Fig. 8a, b, Table 3: Cohesive soil A) where the influence of the stiffness and strength of the cohesive soil, E_{50}^{ref} and c' (Fig. 13a), of the pile–soil interface roughness, R_{inter} (Fig. 13b), and of the pile cross section, d_p and a_p (Fig. 13c), were investigated.

For $q/q_{\text{ult}} \leq 1$, Fig. 13 shows the normalised pressure, p_{mean}/s_u , varying approximately linearly with q/q_{ult} for all parameters investigated which corresponds to in situ measurements documented by [42], who studied a 2×2 pile group supporting a bridge abutment in a 10.5-m-thick cohesive soil layer which was subjected to a load of $q \approx 100$ kPa caused by the backfilling of the abutment. Similar to the model tests the numerical analyses show the normalised pressure, p_{mean}/s_u ,

Table 2 Material properties of the sand (Mohr–Coulomb model)

	$\gamma; \gamma_{\text{sat}}$ kN/m ³	E MPa	ν –	φ' °	c' kPa	ψ °
Upper sand	18; 20	30.0	0.30	40.0	0.1	10.0
Lower sand	18; 20	45.0	0.30	40.0	0.1	10.0

Table 3 Material properties of the cohesive soil as basis for the parametric study (hardening soil model)

Soil	$\gamma; \gamma_{sat}$ kN/m ³	$E_{50}^{ref}=E_{oed}^{ref}$ MPa	E_{ur}^{ref} MPa	p^{ref} kPa	ν_{ur} –	m –	φ' °	c' kPa	ψ °	R_f –
<i>Parametric study with a single pile adjacent to the surface load (Fig. 8a)</i>										
Cohesive soil A	16.0; 16.0	2.0	10.0	100.0	0.20	0.9	20.0	5.0	0	0.9
<i>Parametric study with a different distance between the pile and the surface load and with pile groups (Fig. 8c, Fig. 9)</i>										
Cohesive soil B	18.5; 20.0	6.0	30.0	100.0	0.20	0.8	25.0	10.0	0	0.9
Cohesive soil C	19.0; 19.5	3.0	15.0	100.0	0.20	1.0	20.0	7.5	0	0.9
Cohesive soil D	12.5; 12.5	0.5	2.5	100.0	0.20	1.0	15.0	5.0	0	0.9

Table 4 Material properties of piles and the pile cap (linear elastic)

	$\gamma = \gamma_{sat}$ kN/m ³	E MPa	ν –	R_{inter} °
Piles	24.0	30.0	0.30	0.3–1.0
Pile cap	18.0	60.0	0.30	1.0

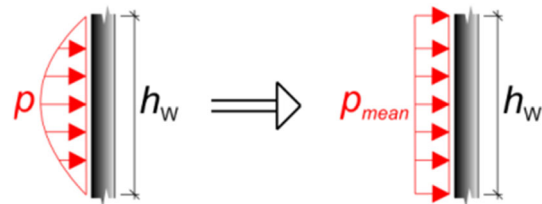
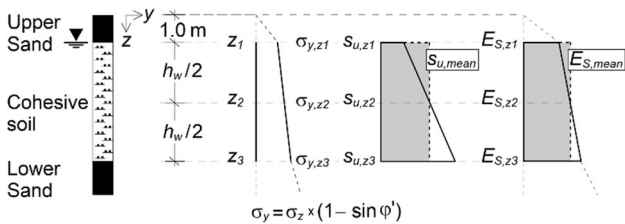


Fig. 12 Mean value of the lateral pressure

(a) Distribution of the minor principal stress σ_y , E_S and s_u in the cohesive soil layer



(b) Numerical simulations of undrained triaxial tests for the calculation of $s_{u,mean}$

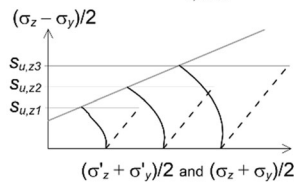


Fig. 10 Estimation of mean values of the constrained modulus E_S and the undrained shear strength s_u for the cohesive soil layer

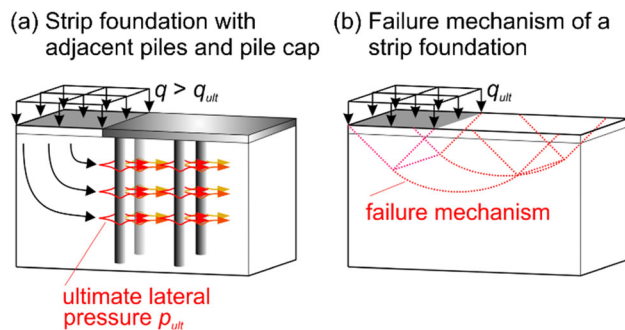


Fig. 11 Surface load q causing the lateral pressure

- decreasing with increasing shear strength (see Figs. 4 and 13a),
- increasing with increasing roughness of the pile–soil interface (see Figs. 5 and 13b).

Moreover, in the numerical analyses the normalised pressure, p_{mean}/s_u ,

- decreased for increasing pile diameter (Fig. 13c),
- was larger for rectangular piles than for circular piles (Fig. 13c),
- increased for increasing cohesive soil stiffness, E_{50}^{ref} , (Fig. 13a).

Investigations carried out with the FE-model indicate that besides the stiffness and shear strength of the cohesive soil, the thickness of the cohesive soil layer, h_w , the pile diameter, d_p , or edge length, a_p , and the magnitude of the load, q , significantly affect the range of influence of the lateral pressure while the shape of the pile cross section, i.e. circular or rectangular, and the roughness of the pile–soil interface are of minor importance [4]. In the investigations of a significantly stiffer layer embedded in the cohesive soil layer, the stiffness ratio and the location of the stiffer layer in particular increase the lateral pressure. Some of the results are discussed below.

Figure 14 shows the variation of the coefficient χ_{dq} with the distance d_q between the pile and the surface load for cohesive soil B, cohesive soil C and cohesive soil D representing clayey soils of varying stiffness and strength (Table 3), for different thickness of the cohesive layer, h_w and for the surface load $q = 0.1 \cdot q_{ult}$ and $q = 0.9 \cdot q_{ult}$, respectively. The factor χ_{dq} is defined as

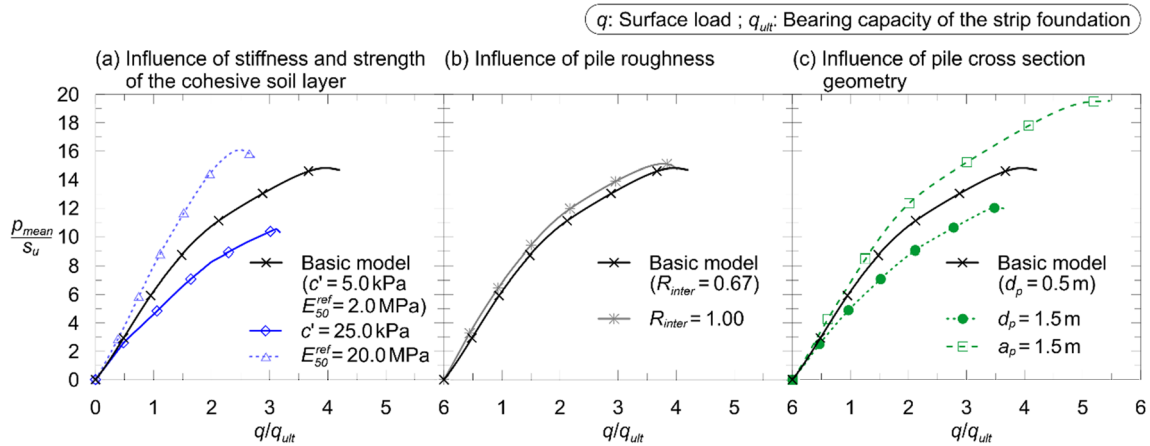


Fig. 13 Numerical study on single piles—variation of the normalised mean pressure acting on piles p/s_u with the normalised surface load q/q_{ult}

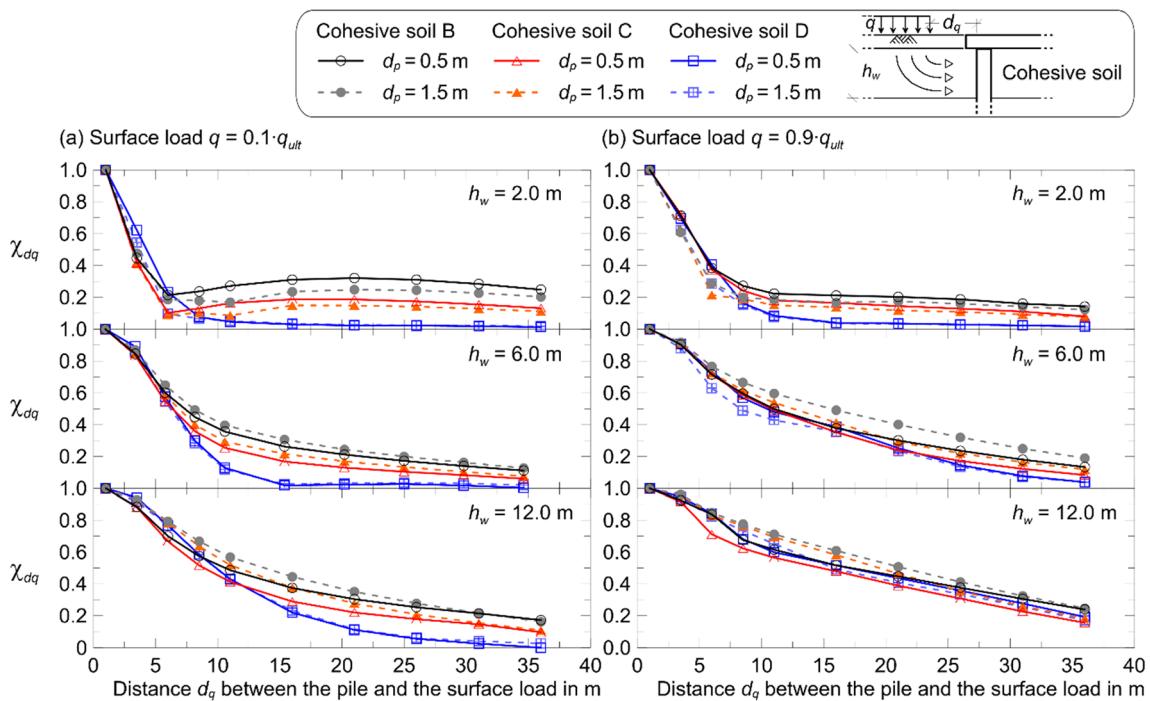


Fig. 14 Numerical study on single piles—variation the factor χ_{dq} (Eq. 4) with the distance d_q between the pile and the surface load q and the thickness of the cohesive soil layer h_w

$$\chi_{dq} = \frac{(p_{mean}/s_u)_d}{(p_{mean}/s_u)_a} \tag{4}$$

where $(p_{mean}/s_u)_d$ is the normalised lateral pressure in a distance d_q from the surface load, and $(p_{mean}/s_u)_a$ is the normalised lateral pressure adjacent to the surface load, i.e. in a distance of $d_q = 1.0$ m.

As an example for the investigations on cohesive soil B and piles with a diameter of $d_p = 0.5$ m and $d_p = 1.5$ m, Fig. 14 leads to the conclusion that higher surface loads generally yield a larger range of influence, i.e. higher values for χ_{dq} . Only for thin cohesive soil layers, e. g.

$h_w = 2.0$ m, a surface load of $q = 0.1 \cdot q_{ult}$ yields higher values for χ_{dq} than $q = 0.9 \cdot q_{ult}$, at least at distances larger than 10 m. This is possibly caused by the fact that the area of influence is limited to the geometry of the already developing failure mechanism in the cohesive soil, which has only a small range due to the comparatively small layer thickness.

Furthermore, the following conclusions can be drawn from the results presented in Fig. 14:

- χ_{dq} increases for increasing thickness of the cohesive soil layer, h_w .

- χ_{dq} increases for stiffer soils, i.e. with higher stiffness and shear strength, although this effect is less pronounced for increasing thickness of the cohesive soil layer.
- For a thickness of the cohesive soil layer of $h_w \geq 6$ m, a pile diameter of $d_p = 1.5$ m yields higher values for χ_{dq} , while for $h_w = 2$ m, the piles with $d_p = 0.5$ m show higher values for χ_{dq} .

3.4 Results of the numerical study for pile groups

The group factor χ_{GP} relates the normalised lateral pressure of a pile within a pile group, $(p_{\text{mean}}/s_u)_G$, to the normalised lateral pressure of a single pile, $(p_{\text{mean}}/s_u)_S$:

$$\chi_{GP} = \frac{(p_{\text{mean}}/s_u)_G}{(p_{\text{mean}}/s_u)_S} \quad (5)$$

Preliminary investigations carried out with the FE-model shown in Fig. 9 indicated that the factor χ_{GP} in particular depends on the stiffness and the shear strength of the soil, the pile diameter or edge length and the roughness of the pile–soil interface [4]. Piles with a rectangular cross section always yield smaller group factors than piles with a circular cross section provided $a_p = d_p$. The thickness of the cohesive soil layer, h_w , has a negligible influence on the group factor. Since group effects proved to be more significant for higher surface loads the results presented subsequently were derived for $q = q_{\text{ult}}$. The material parameters applied for the cohesive soil are summarised in Table 3.

Generally, the further back the piles are located within the group the smaller the lateral pressure and the group factor χ_{GP} will become. This can be attributed to the shielding effect of the piles standing in front of them on the one hand and to the greater distance to the surface load on the other hand. For pile rows perpendicular to the soil movement (Fig. 9b, R1 to R5), the piles located at the edge of the group (Fig. 9b, pile type A) show a higher group factor χ_{GP} than the piles located inside the group (Fig. 9b, pile type I). Selected results are presented in Fig. 15 with the group factor χ_{GP} plotted versus the number of the pile rows perpendicular to the soil movement for the pile spacing $s = 3 \cdot d_p$.

For the cohesive soil B, Fig. 15a shows the influence of the size of the pile group on the group factor χ_{GP} for pile type A with a diameter of $d_p = 0.5$ m and an interface roughness of $R_{\text{inter}} = 1.00$. For each row, the pile group with the smallest number of piles yields the highest group factor χ_{GP} . An upper limit curve (Fig. 15a, curve “Max.”) can be derived from this maximum group factor. All remaining results presented in Fig. 15b, c and d are based

on such an upper limit curve, determined in each case from pile groups comprising 2×2 , 3×3 , 4×4 and 5×5 piles.

For pile row R1 in ultimate vicinity to the surcharge load the piles with $d_p = 1.5$ m show higher group factors than the piles with $d_p = 0.5$ m, while for all other pile rows, the opposite holds true (Fig. 15b). Figure 15c compares the group factor χ_{GP} of pile types A and I and for soil types cohesive soil B, cohesive soil C and cohesive soil D (Table 3) with pile type A generally showing higher group factors than pile type I. For higher stiffness and shear strength, the group factor becomes gradually higher. However, this effect is not as significant as the variation of the group factor resulting from different pile positions.

The roughness of the pile–soil interface only has a small influence on the group factors as indicated in Fig. 15d. For pile rows close to the surface load (R1, R2) the piles with a smoother surface ($R_{\text{inter}} = 0.33$) show higher group factors while for pile rows further away (R4, R5) rough surfaces ($R_{\text{inter}} = 1.00$) give marginally higher values. This is in agreement with the results achieved by [33] for square pile groups in undrained soil who observed a negligible influence of pile–soil roughness on the group lateral limiting pressure if piles in large groups are spaced closely together.

Figure 16 extends the investigations on the group effects on the lateral pressure with the group factor χ_{GP} plotted versus the number of the pile rows perpendicular to the soil movement for pile groups comprising 2×2 , 2×3 , 3×3 , 4×3 , 4×4 and 5×5 piles and pile spacings between $s = 3 \cdot d_p$ and $s = 9 \cdot d_p$. Parameters varied in the study were the soil type (Cohesive soil B, Cohesive soil C and Cohesive soil D according to Table 3), the pile diameter ($d_p = 0.5$ m; $d_p = 1.5$ m) and the roughness of the pile–soil interface ($R_{\text{inter}} = 0.33$; $R_{\text{inter}} = 1.00$), while the thickness of the cohesive soil layer was held constant at $h_w = 6.0$ m. The values for the group factor χ_{GP} given in Fig. 16 represent the maximum values derived from the parametric study.

From the results presented in Fig. 16, it is possible to draw the following conclusions:

- For pile spacings $s \geq 9 \cdot d_p$, the piles in row R1 adjacent to the surface load behave as a comparable single pile, i.e. $\chi_{GP} = 1.0$.
- For pile spacings $s < 9 \cdot d_p$, the lateral pressure acting on a group pile is smaller than the lateral pressure on a comparable single pile, $\chi_{GP} < 1.0$.
- As could be expected, for larger piles spacings group effects diminish. However, when looking at pile rows orientated parallel to the soil movement (or for example comparing the same pile type in row R1 and row R5) the increasing distance between the piles in the back rows and the surface load yields a decrease in the group

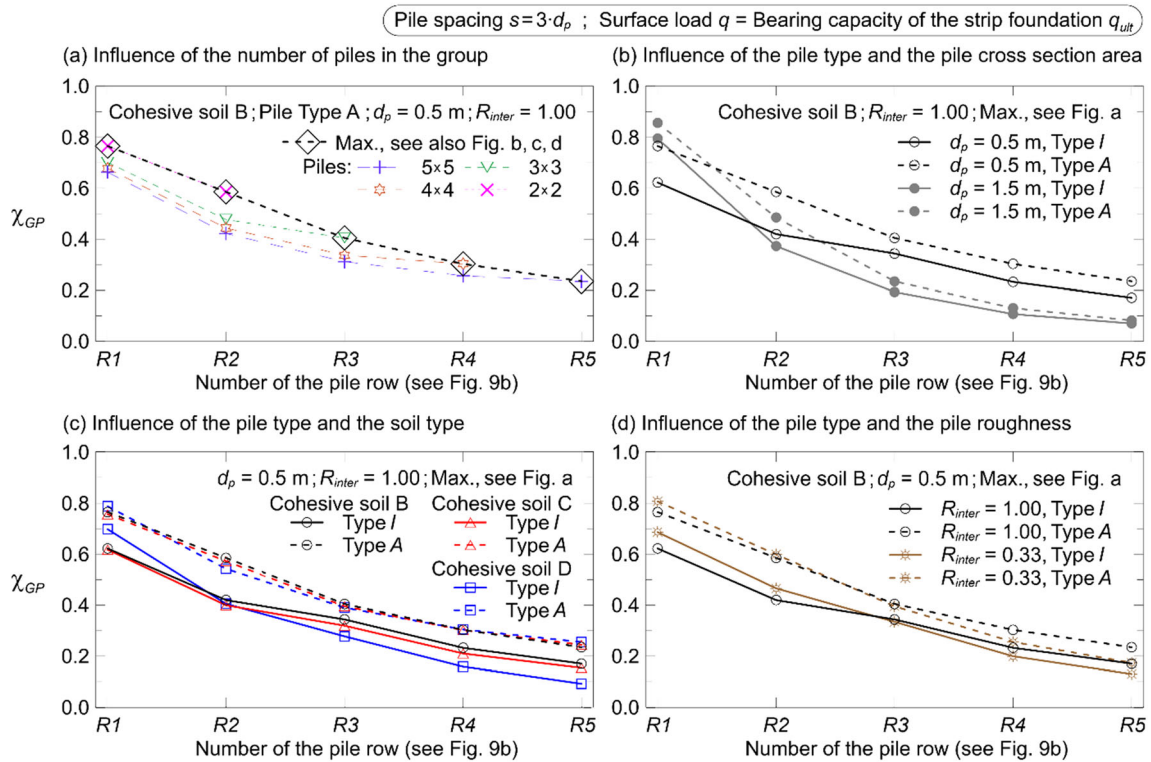


Fig. 15 Numerical study on pile groups—variation the factor χ_{GP} (Eq. 5) with the pile position relative to the surface load (Fig. 9b) for piles arranged one behind the other in rows

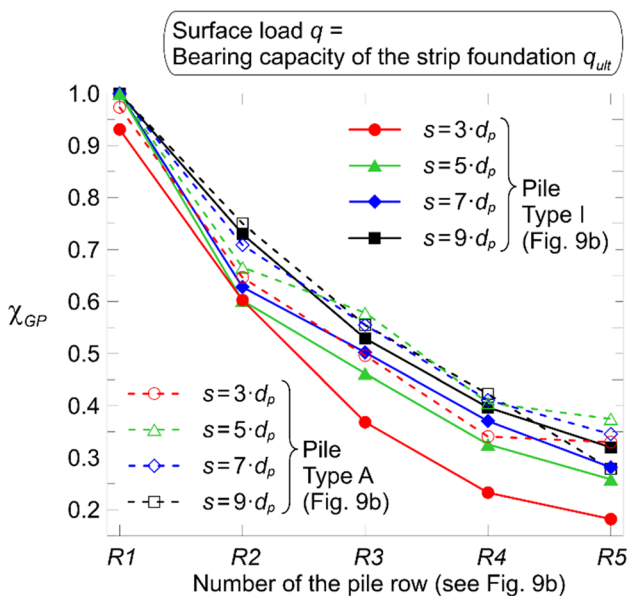


Fig. 16 Numerical study on pile groups—variation of factor χ_{GP} (Eq. 5) with the pile position relative to the surface load (Fig. 9): Influence of the pile spacing for piles arranged one behind the other in rows as well as in staggered rows

factor which could be interpreted as an increase in group effects.

- Model tests by [7] not presented in the scope of this paper show that with decreasing pile spacing the lateral pressure on the piles is decreasing for front row piles as well as for back row piles. In the numerical study, this effect is reflected when comparing the results for row R1 (front row pile) for $s = 3 \cdot d_p$ ($\chi_{GP} \approx 0.93$) and $s = 9 \cdot d_p$ ($\chi_{GP} = 1.0$). The piles in the back rows R2 to R5 are shielded by the front row piles, while at the same time, the movement of the soil around the front row piles is obstructed by the back row piles.

4 Approach for the analysis of piles subjected to lateral pressure

Based on the results of the numerical parametric study [4] developed an improved approach for the analysis of piles subjected to lateral pressure to overcome the limitations in Recommendations on Piling (DGGT 2014 [15]) discussed by [5]. The approach modifies Eq. (1) as follows:

$$\begin{aligned} P_{ult} &= (6 \cdot \chi \cdot s_u \cdot \mu + \Delta p_t) \cdot d_p \quad \text{or} \\ P_{ult} &= (6 \cdot \chi \cdot s_u \cdot \mu + \Delta p_t) \cdot a_p \end{aligned} \tag{6}$$

where: 6 is the ratio of the normalised pressure, p_{mean}/s_u , in the basic element model shown in Fig. 7a (circular single pile) with the parameters in Tables 2, 3 and 4, s_u is the

undrained shear strength of the cohesive soil layer, μ is the degree of utilisation of the strip foundation (Fig. 11b), Δp_t is the lateral pressure acting on the pile due to creep deformations, d_p is the pile diameter, a_p is the edge length of the pile and, χ is the combination of several coefficients:

$$\chi = \chi_{su} \cdot \chi_{hw} \cdot \chi_{Es} \cdot \chi_d \cdot \chi_{SE} \cdot \chi_{dq} \cdot \chi_{GP} \quad (7)$$

where: χ_{su} is the coefficient for the undrained shear strength s_u (see Table 5), χ_{hw} is the coefficient for the thickness of the cohesive soil layer h_w (see Table 6), χ_{Es} is the coefficient for the confined stiffness modulus of the cohesive soil layer E_S (see Table 7), χ_d is the coefficient for the shape and the cross-section area of the pile (see Table 8), χ_{SE} is the coefficient for the effect of a significantly stiffer layer embedded in the cohesive soil layer (see Table 9), χ_{dq} is the coefficient for the distance between the pile and the surface load d_q (see Table 10), χ_{GP} is the coefficient for pile group effects (see Table 11 and Fig. 16).

The coefficients represent the upper limits derived from the parametric studies. In the following Table 5 to Table 11, intermediate values can be interpolated linearly. The system configuration with the definition of the relevant parameters is shown in Figs. 7 and 9b.

The parameter λ in Table 9 is calculated as follows:

$$\lambda = \frac{E_{S,s}}{E_{S,c}} \quad (8)$$

where: $E_{S,s}$ is the confined stiffness modulus of the significantly stiffer layer embedded in the cohesive soil layer, $E_{S,c}$ is the confined stiffness modulus of the cohesive soil layer.

The lateral pressure Δp_t acting on the pile due to creep deformations can be approximated for a time period of 50 years as follows:

$$p_t = 700 \cdot I_v \quad (9)$$

where: I_v is the viscosity index according to [18, 22]

To further investigate the parameter Δp_t , future research may incorporate more sophisticated visco-hypoplastic models such as, e.g. the AVISA model [36].

To establish the degree of utilisation, available analytical approaches to establish the stability, e.g. of a strip foundation (e.g. [29]) or a slope (e.g. [9]) can be applied.

Table 5 Coefficient χ_{su}

s_u	≤ 5 kPa	10 kPa	≥ 30 kPa
χ_{su} for $h_w \leq 6$ m	1.35	1.00	0.90
χ_{su} for $h_w > 6$ m	1.00	1.00	1.30

Table 6 Coefficient χ_{hw}

h_w	≤ 4 m	≥ 12 m
χ_{hw}	1.30	0.80

As documented by [24], this new approach has since replaced the approach documented in the Recommendations on Piling (DGGT 2014 [15]). For a detailed documentation, it is referred to [4] and the upcoming 3rd edition of the Recommendations on Piling of the DGGT.

5 Summary and conclusions

This paper documents selected results of a research project investigating the influencing variables on the lateral pressure on piles by means of $1 \times g$ model tests and numerical studies. As a first step, a total of 40 model tests were carried out to experimentally determine main parameters influencing the lateral pressure. On the basis of these model tests and large-scale and centrifuge tests documented in the literature, a finite element model was developed in [4]. The finite element model was then used for a parametric numerical study to systematically investigate the influence of a surcharge load on the lateral pressure acting on an adjacent pile group.

Key results derived from the model tests and the parametric numerical study can be summarised as follows:

- The lateral pressure increases with
 - increasing shear strength of the cohesive soil,
 - increasing stiffness of the cohesive soil and
 - increasing roughness of the pile–soil interface.
- The lateral pressure decreases with
 - increasing pile diameter and
 - increasing distance between the pile and the surface load.
- The lateral pressure acting on group piles is smaller than the lateral pressure on a comparable single pile. In general, the lateral pressure decreases with decreasing pile spacing.
- For piles at the back of a pile group, the lateral pressure is smaller than for piles in the front row closer to the pressure inducing surface load, i.e. “leeward” to the loading.

Based on the results of the numerical parametric study with in total more than 1400 configurations for single piles and pile groups investigated, coefficients to quantify the

Table 7 Coefficient χ_E

E_S	$\leq 0.5 \text{ MN/m}^3$	1.5 MN/m^3	3.0 MN/m^3	$\geq 7 \text{ MN/m}^3$
χ_E for $h_w < 4 \text{ m}$	1.00	1.40	1.55	1.55
χ_E for $h_w \geq 4 \text{ m}$	1.00	1.25	1.30	1.45

Table 8 Coefficient χ_d

$d_p; a_p$	0.3 m	0.5 m	1.5 m	3.0 m
χ_d for the edge length of a pile a_p	1.41	1.37	1.15	0.82
χ_d for the diameter of a pile d_p	1.03	1.00	0.86	0.65

Table 9 Coefficient χ_{SE} in dependency of λ (Eq. 8)

Effect of stiffness	$\lambda \leq 3$	$3 < \lambda \leq 35$		$35 < \lambda \leq 150$	
Depth of the stiffer layer embedded in the cohesive soil layer		$z_{SE} = 1 \text{ m}$	$z_{SE} \geq 5 \text{ m}$	$z_{SE} = 1 \text{ m}$	$z_{SE} \geq 9 \text{ m}$
χ_{SE}	1.00	1.50	1.00	1.90	1.00

Table 10 Coefficient χ_{dq}

Distance	$d_q < 2.5$	$d_q = 10$			$d_q \geq 40$		
Thickness of the cohesive soil layer		$h_w \leq 2$	$2 < h_w \leq 6$	$h_w > 6$	$h_w \leq 2$	$2 < h_w \leq 6$	$h_w > 6$
χ_{dq}	1.00	0.35	0.65	0.75	0.35	0.15	0.20

Table 11 Coefficient χ_{GP}

Pile row	$R1$	$R2$	$R3$	$R4$	$\geq R5$
Pile type I	1.00	0.73	0.52	0.39	0.32
Pile type A	1.00	0.75	0.58	0.42	0.37

influence of the above mentioned parameters were established. Using these coefficients, an improved method was developed for the analysis of piles subjected to lateral pressure which as documented by [24] has since replaced the approach documented in the Recommendations on Piling (DGGT 2014 [15]).

Funding Open Access funding enabled and organized by Projekt DEAL.

Data availability statement Data will be made available on reasonable request.

Declarations

Conflict of interest The authors declare that they have no financial interests or non-financial interests directly or indirectly related to the work submitted for publication.

Open Access This article is licensed under a Creative Commons Attribution 4.0 International License, which permits use, sharing, adaptation, distribution and reproduction in any medium or format, as long as you give appropriate credit to the original author(s) and the source, provide a link to the Creative Commons licence, and indicate if changes were made. The images or other third party material in this article are included in the article's Creative Commons licence, unless indicated otherwise in a credit line to the material. If material is not included in the article's Creative Commons licence and your intended use is not permitted by statutory regulation or exceeds the permitted use, you will need to obtain permission directly from the copyright holder. To view a copy of this licence, visit <http://creativecommons.org/licenses/by/4.0/>.

References

1. Al-Kafaji I (2013) Formulation of a dynamic material point method (MPM) for geomechanical problems. Dissertation, University of Stuttgart, Germany

2. Aschrafi J (2019) Beitrag zur Seitendruckbeanspruchung von Pfählen in bindigen Böden. Dissertation, University of Stuttgart, Germany
3. Aschrafi J, Giridharan S, Moormann C (2018) Group Effects for pile rows under passive lateral loading. In: DFI-EFFC international conference on deep foundations and ground improvement, Rome, Italy, pp 189–198
4. Bauer J (2016) Seitendruck auf Pfahlgründungen in bindigen Böden infolge quer zur Pfahlachse wirkender Bodenverschiebungen. Dissertation, University of Kassel, Germany
5. Bauer J, Kempfert H-G (2018) Untersuchungen zum Seitendruck auf Pfahlgründungen in bindigen Böden. Bauingenieur 93(12):473–481. <https://doi.org/10.37544/0005-6650-2018-12>
6. Bauer J, Kempfert H-G, Reul O (2014) Lateral pressure on piles due to horizontal soil movement—Ig model tests on single piles and pile rows. In: Proceedings of the 8th international conference on physical modelling in Geotechnique, Perth, Australia, pp 839–845
7. Bauer J, Kempfert H-G, Reul O (2016) Lateral pressure on piles due to horizontal soil movement. Int J Phys Model Geotech 16(4):173–184. <https://doi.org/10.1680/jphmg.15.00005>
8. Bauer J, Reul O (2015) Experimental and numerical studies on the lateral pressure acting on piles due to horizontal soil movements. In: Proceedings of the XVI ECSMGE, Edinburgh, Scotland, pp 3803–3808
9. Bishop AW (1955) The use of the slip circle in the stability analysis of slope. Geotechnique 5(1):129–150. <https://doi.org/10.1680/geot.1955.5.1.7>
10. Bransby F (1995) Piled foundations adjacent to surcharge loads. Dissertation, University of Cambridge, UK
11. Brinkgreve RBJ, Kumaraswamy S, Swolfs WM (2016). Plaxis 2016. Plaxis bv, Delft
12. Chen CY, Martin GR (2002) Soil-structure interaction for landslide stabilizing piles. Comput Geotech 29(5):363–386. [https://doi.org/10.1016/S0266-352X\(01\)00035-0](https://doi.org/10.1016/S0266-352X(01)00035-0)
13. Chen LT (1994) The effect of lateral soil movements on pile foundation. Dissertation, University of Sydney, Australia
14. De Beer EE (1977) The effects of horizontal loads on piles, due to surcharge or seismic effects. In: Proceedings of the IX ICSMFE, Speciality Session, Tokyo, Japan, pp 547–558
15. Deutsche Gesellschaft für Geotechnik (DGGT; German Geotechnical Society) (2014) Recommendations on Piling (EA-Pfähle). Translation of the 2nd edn. of the EA-Pfähle, Verlag Ernst & Sohn
16. DIN 1054 2010-12 (2010) Subsoil—verification of the safety of earthworks and foundations—supplementary rules to DIN EN 1997-1. Beuth Verlag, Berlin
17. DIN EN 1997-1:2009-09 (2009) Eurocode 7: Geotechnical design—part 1: general rules; German version EN 1997-1:2004 + AC:2009. Beuth Verlag, Berlin
18. Gudehus G, Leinenkugel H-J (1978) Fließdruck und Fließbewegung in bindigen Böden: Neue Methoden. In: Vorträge zur Baugrundtagung. Essen, Germany, pp 411–429
19. Hamad F (2016) Formulation of the axisymmetric SPDI with application to pile driving in sand. Comput Geotech 74:141–150. <https://doi.org/10.1016/j.compgeo.2016.01.003>
20. Jeong S, Seo D, Kim Y (2009) Numerical analysis of passive pile groups in offshore soft deposits. Comput Geotech 36(7):1164–1175. <https://doi.org/10.1016/j.compgeo.2009.05.003>
21. Knappett JA, Mohammadi S, Griffin C (2010) Lateral spreading forces on bridge piers and pile caps in laterally spreading soil: effect of angle of incidence. J Geotech Geoenviron Eng 136(12):1589–1599. [https://doi.org/10.1061/\(ASCE\)GT.1943-5606.0000387](https://doi.org/10.1061/(ASCE)GT.1943-5606.0000387)
22. Leinenkugel HJ (1976): Deformations- und Festigkeitsverhalten bindiger Erdstoffe. Experimentelle Ergebnisse und ihre physikalische Bedeutung. Dissertation, University of Karlsruhe, Germany
23. Miao LF, Goh ATC, Wong KS, The CI (2008) Ultimate soil pressure for pile groups in soft clay subjected to lateral soil movements. DFI J 2(1):42–51. <https://doi.org/10.1179/dfi.2008.005>
24. Moormann C (2021) Jahresbericht 2020 des Arbeitskreises „Pfähle“ der Deutschen Gesellschaft für Geotechnik (DGGT). Bautechnik 98(2):163–186. <https://doi.org/10.1002/bate.202100005>
25. Mühl A, Thá PC, Glockner A, Röder K (2011) Instrumentation and monitoring of a full-scale test on pile foundations for overhead bridge cranes. In: Proceedings of the 8th international symposium on field measurements in geomechanics, Berlin, Germany, pp 1–20
26. Ong DEL, Leung CF, Chow YK (2009) Behavior of pile groups subject to excavation-induced soil movement in very soft clay. J Geotech Geoenviron Eng 135(10):1462–1474. [https://doi.org/10.1061/\(ASCE\)GT.1943-5606.0000095](https://doi.org/10.1061/(ASCE)GT.1943-5606.0000095)
27. Pan JL, Goh ATC, Wong KS, Teh CI (2000) Model tests on single piles in soft clay. Can Geotech J 37(4):890–897. <https://doi.org/10.1139/t00-001>
28. Pan JL, Goh ATC, Wong KS, Teh CI (2002) Ultimate soil pressures for piles subjected to lateral soil movements. J Geotech Geoenviron Eng 128(6):530–535. [https://doi.org/10.1061/\(ASCE\)1090-0241\(2002\)128:6\(530\)](https://doi.org/10.1061/(ASCE)1090-0241(2002)128:6(530))
29. Prandtl L (1920) Über die Härte plastischer Körper. Nachrichten von der Königlichen Gesellschaft der Wissenschaften zu Göttingen, Mathematisch-Physikalische Klasse 1:74–85
30. Randolph MF, Houlsby GT (1984) The limiting pressure on a circular pile loaded laterally in cohesive soil. Géotechnique 34(4):613–623. <https://doi.org/10.1680/geot.1984.34.4.613>
31. Reul O, Bauer J, Niemann C (2014) Numerical study on the bearing behaviour of pile groups subjected to lateral pressure due to soil movements. Geot Eng J SEAGS AGSSEA 45(2):106–114
32. Schenk W, Smolczyk H-U (1966) Pfahlroste, Berechnung und Ausbildung. In: Grundbau-Taschenbuch, 2nd edn. Ernst & Sohn, Berlin, Germany, pp 658–715
33. Sheil BB (2021) Lateral limiting pressure on square pile groups in undrained soil. Géotechnique 71(4):279–287. <https://doi.org/10.1680/jgeot.18.P.118>
34. Soumaya B (2005) Setzungsverhalten von Flachgründungen in normalkonsolidierten bindigen Böden. Dissertation, University of Kassel, Germany
35. Stewart DP, Jewell JR, Randolph MF (1994) Design of piled bridge abutments on soft clay for loading from lateral soil movements. Géotechnique 42(2):277–296. <https://doi.org/10.1680/geot.1994.44.2.277>
36. Tafili M, Triantafyllidis T (2020) AVISA: anisotropic visco-ISA model and its performance at cyclic loading. Acta Geotech 15(2):2395–2413. <https://doi.org/10.1007/s11440-020-00925-9>
37. Tong L, Li H, Ha S, Liu S (2022) Lateral bearing performance and mechanism of piles in the transition zone due to pit-in-pit excavation. Acta Geotech 17(8):1935–1948. <https://doi.org/10.1007/s11440-021-01341-3>
38. Uriel S, Uriel AO, Oteo CS, Canizo L (1976) Behaviour of precast piles under lateral pressures at a shipbuilding site. In: Proceedings of the 6th European conference of soil mechanics and geotechnical engineering, Wien, Austria, pp 585–590
39. Wenz KP (1963) Über die Größe des Seitendrucks auf Pfähle in bindigen Erdstoffen. Dissertation, University of Karlsruhe, Germany
40. Wenz KP (1972) Seitendruck auf Pfähle in weichen bindigen Erdstoffen. In: Vorträge zur Baugrundtagung, Stuttgart, Germany, pp 681–690

41. White DJ, Take WA, Bolton MD (2003) Soil deformation measurement using particle image velocimetry (PIV) and photogrammetry. *Géotechnique* 53(7):619–631. <https://doi.org/10.1680/geot.2003.53.7.619>
42. Wolf A, Thamm B (1988) Messungen des Seitendrucks auf Großbohrpfähle eines Brückenwiderlagers. *Bautechnik* 65(3):80–87

Publisher's Note Springer Nature remains neutral with regard to jurisdictional claims in published maps and institutional affiliations.